High Step-Up Converter With Three-Winding Coupled Inductor for Fuel Cell Energy Source Applications

Kuo-Ching Tseng, Jang-Ting Lin, and Chi-Chih Huang

***Abstract*—This paper presents a high step-up converter for fuel cell energy source applications. The proposed high step-up dc–dc converter is devised for boosting the voltage generated from fuel cell to be a 400-V dc-bus voltage. Through the three-winding coupled inductor and voltage doubler circuit, the proposed converter achieve high step-up voltage gain without large duty cycle. The passive lossless clamped technology not only recycles leakage energy to improve efficiency but also alleviates large voltage spike to limit the voltage stress. Finally, the fuel cell as input voltage source 60–90 V integrated into a 2-kW prototype converter was implemented for performance verification. Under output voltage 400-V operation, the highest efficiency is up to 96.81%, and the full-load efficiency is 91.32%.**

***Index Terms*—Coupled inductor, fuel cell energy source applications, high step-up converter.**

I. Introduction

RECENTLY, the cost increase of fossil fuel and new regulations of CO_2 emissions have strongly increased the interests in renewable energy sources. Hence, renewable energy sources such as fuel cells, solar energy, and wind power have been widely valued and employed. Fuel cells have been considered as an excellent candidate to replace the conventional diesel/gasoline in vehicles and emergency power sources. Fuel cells can provide clean energy to users without CO_2 emissions. Due to stable operation with high-efficiency and sustainable/renewable fuel supply, fuel cell has been increasingly accepted as a competently alternative source for the future [1], [2]. The excellent features such as small size and high conversion efficiency make them valuable and potential. Hence, the fuel cell is suitable as power supplies for energy source applications [3]–[16].

Generally speaking, a typical fuel cell power supply system containing a high step-up converter is shown in Fig. 1. The generated voltage of the fuel cell stack is rather low. Hence, a high step-up converter is strongly required to lift the voltage for applications such as dc microgrid, inverter, or battery.

Manuscript received July 24, 2013; revised October 23, 2013 and January 19, 2014; accepted February 22, 2014. Date of publication March 11, 2014; date of current version October 7, 2014. Recommended for publication by Associate Editor S. Williamson.

The authors are with the Department of Electronics Engineering, National Kaohsiung First University of Science and Technology, Kaohsiung 811, Taiwan (e-mail: jerry@nkfust.edu.tw; seikobaby@gmail.com; u0052809@nkfust.edu.tw).

Digital Object Identifier 10.1109/TPEL.2014.2309793

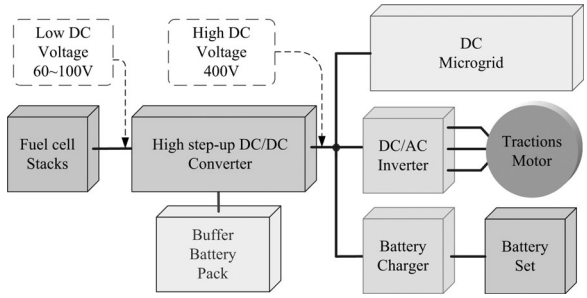

Fig. 1. Fuel cell power supply system with high step-up converter.

Ideally, a conventional boost converter is able to achieve high step-up voltage gain with an extreme duty cycle. In practice, the step-up voltage gain is limited by effects of the power switch, rectifier diode, and the resistances of the inductors and capacitors. In addition, the extreme duty cycle may result in a serious reverse-recovery problem and conduction losses. A flyback converter is able to achieve high step-up voltage gain by adjusting the turns ratio of the transformer winding [17], [18]. However, a large voltage spike leakage energy causes may destroy the main switch. In order to protect the switch devices and constrain the voltage spike, a high-voltage-rated switch with high on-state resistance $(R_{\mathrm{DS\text{-}ON}})$ and a snubber circuit are usually adopted in the flyback converter, but the leakage energy still be consumed. These methods will diminish the power conversion efficiency [19]–[21]. In order to increase the conversion efficiency and voltage gain, many technologies such as zero-voltage switching (ZVS), zero-current switching (ZCS), coupled inductor, active clamp, etc. [22]–[24] have been investigated. Some high step-up voltage gain can be achieved by using switched-capacitor and voltage-lift techniques [25]–[28], although switches will suffer high current and conduction losses. In recent years, coupled-inductor technology with performance of leakage energy recycle is developed for adjustable voltage gain; thus, many high step-up converters with the characteristics of high voltage gain, high efficiency, and low voltage stress have been presented [29]–[39]. In addition, some novel high step-up converters with three-winding coupled inductor have also been proposed, which possess more flexible adjustment of voltage conversion ratio and voltage stress [37], [39]. In this paper, the proposed high step-up converter designed for fuel cell energy source applications is shown in Fig. 2. The fuel cell with inertia characteristics as main power source cannot respond to load dynamics well. Therefore, lithium iron phosphate can be an excellent candidate for secondary source to react to fast

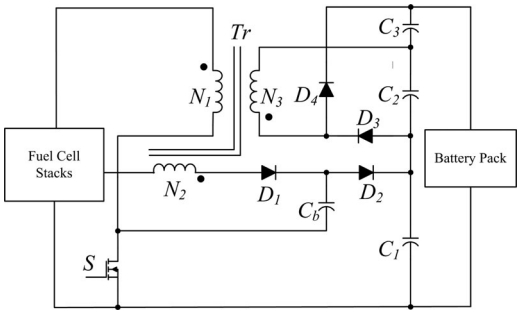

Fig. 2. Proposed high step-up converter.

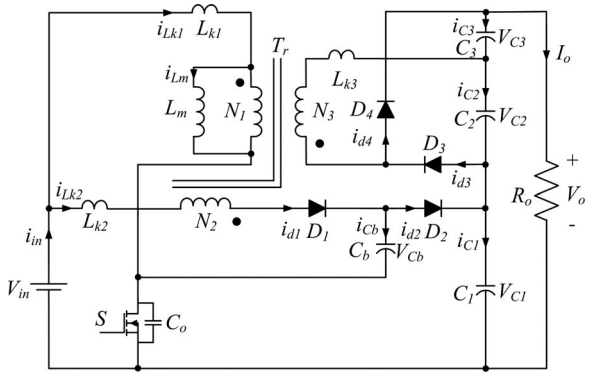

Fig. 3. Equivalent circuit of the proposed converter.

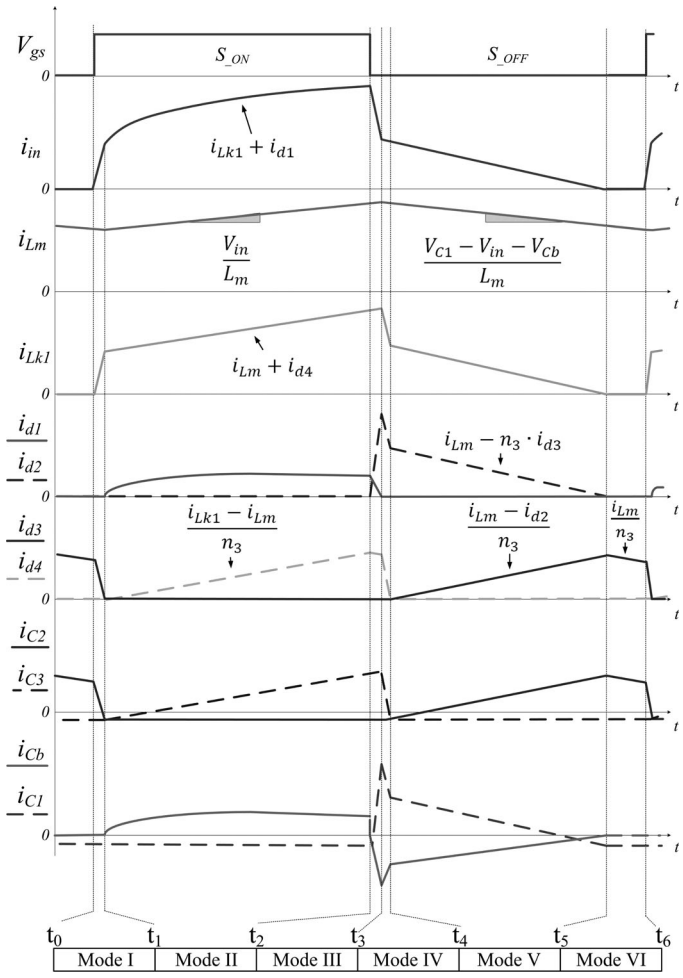

Fig. 4. Steady-state waveforms in CCM operation.

dynamics and contribute to load peaking. The proposed converter with fuel cell input source is suitable to operate in continuous conduction mode (CCM) because the discontinuous conduction mode operation results in large input current ripple and high peak current, which make the fuel cell stacks difficult to afford.

II. Operating Principle of the Proposed Converter

The proposed converter employs a switched capacitor and a voltage-doubler circuit for high step-up conversion ratio. The switched capacitor supplies an extra step-up performance; the voltage-doubler circuit lifts of the output voltage by increasing the turns ratio of coupled-inductor. The advantages of proposed converter are as follows:

1) through adjusting the turns ratio of coupled inductor, the proposed converter achieves high step-up gain that renewable energy systems require;
2) leakage energy is recycled to the output terminal, which improves the efficiency and alleviates large voltage spikes across the main switch;
3) due to the passive lossless clamped performance, the voltage stress across main switch is substantially lower than the output voltage;
4) low cost and high efficiency are achieved by adopting low-voltage-rated power switch with low $R_{\mathrm{DS\text{-}ON}}$;
5) by using three-winding coupled inductor, the proposed converter possesses more flexible adjustment of voltage conversion ratio and voltage stress on each diode.

The equivalent circuit of the proposed converter shown in Fig. 3 is composed of a coupled inductor T_r, a main power switch S, diodes D_1, D_2, D_3, and D_4, the switched capacitor C_b, and the output filter capacitors C_1, C_2, and C_3. L_m is the magnetizing inductor and L_{k1}, L_{k2}, and L_{k3} represent the leakage inductors. The turns ratio of coupled inductor n_2 is equal to N_2/N_1, and n_3 is equal to N_3/N_1, where N_1, N_2, and N_3 are the winding turns of coupled inductor.

The steady-state waveforms of the proposed converter operating in CCM are depicted in Fig. 4. The each operating modes is shown in Fig. 5.

Mode I [t_0, t_1]: During this interval, the switch S is turned ON at t_0. The diodes D_1, D_2, and D_4 are reverse biased. The path of current flow is shown in Fig. 5(a). The primary leakage inductor current i_{Lk1} increases linearly, and the energy stored in magnetizing inductance still transfers to the load and output capacitor C_2 via diode D_3.

Mode II [t_1, t_2]: During this interval, the switch S is still in the turn-on state. The diodes D_1 and D_4 are forward biased; diodes D_2 and D_3 are reverse biased. The path of current flow is shown in Fig. 5(b). The dc source V_{in} still charges into the magnetizing inductor L_m and leakage inductor L_{k1}, and the currents through these inductors rise linearly. Some of the energy from dc source V_{in} transfer to the secondary side of the coupled inductor to charge the capacitor C_3. The switched capacitor C_b is charged by the *LC* series circuit.

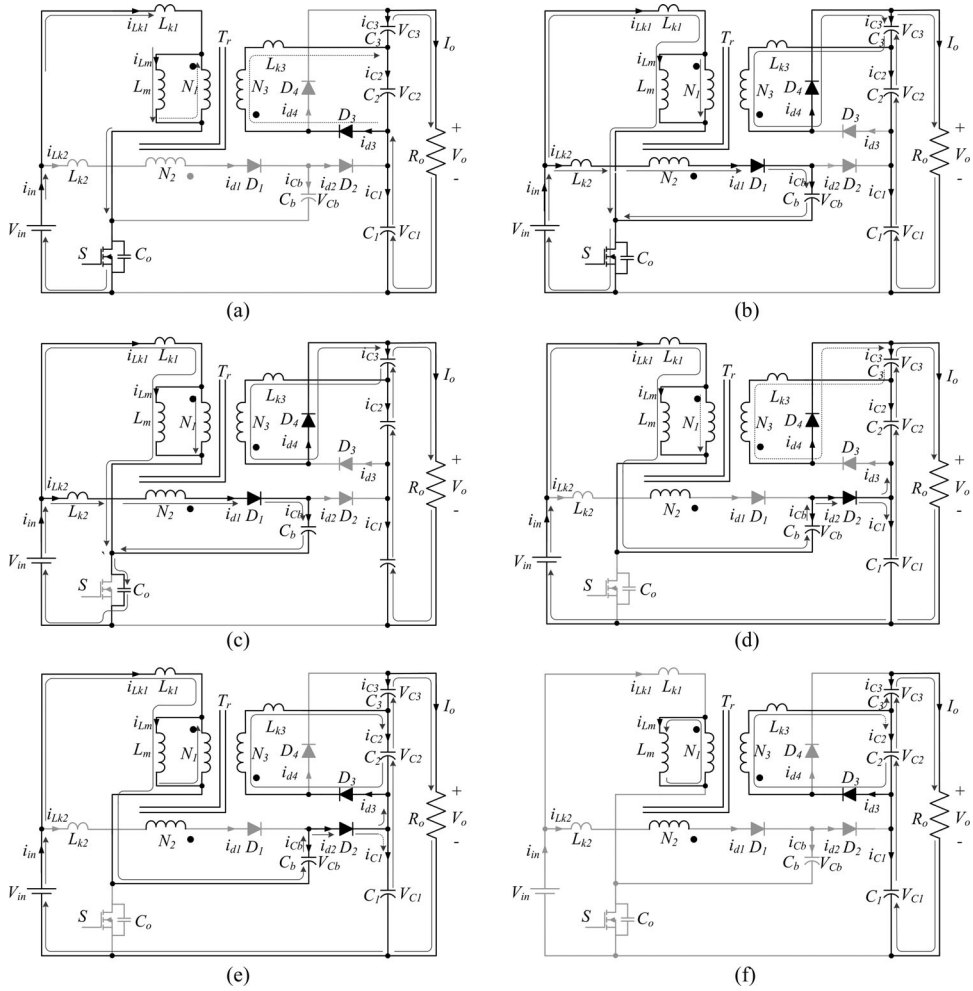

Fig. 5. CCM operating modes of the proposed converter. (a) Mode I $[t_0, t_1]$. (b) Mode II $[t_1, t_2]$. (c) Mode III $[t_2, t_3]$. (d) Mode IV $[t_3, t_4]$. (e) Mode V $[t_4, t_5]$. (f) Mode VI $[t_5, t_6]$.

Mode III [t_2, t_3]: During this interval, the switch S is turned OFF at t_2. Diodes D_1 and D_4 are still forward biased; diodes D_2 and D_3 are reverse biased. The path of current flow is shown in Fig. 5(c). The magnetizing current and *LC* series current charge the parasitic capacitor C_o of the MOSFET.

Mode IV [t_3, t_4]: During this interval, S is still in the turn-off state. The diodes D_1, D_2, and D_4 are forward biased. The diode D_3 is reverse biased. The current-flow path is shown in Fig. 5(d). The current i_{d4} charges the output capacitor C_3 and decreases linearly. The total voltage of $V_{\rm in}+V_{Lm}+V_{Cb}$ is charging to clamped capacitor C_1, and some of the energy is supplied to the load.

Mode V [t_4, t_5]: During this interval, switch S is still in the turn-off state. The diodes D_1 and D_4 are turned OFF; the diodes D_2 and D_3 are forward biased. The current-flow path is shown in Fig. 5(e). The energy of the primary side still charges to the clamped capacitor C_1 and supplies energy to the load. Some of the energy from dc source $V_{\rm in}$ is transferred to the secondary side of the coupled inductor to charge the capacitor C_2, and the current i_{d3} increases linearly.

Mode VI [t_5, t_6]: During this interval, switch S is still in the turn-off state. The diodes D_1, D_2, and D_4 are reverse biased; the diode D_3 is forward biased. The current-flow path is shown in Fig. 5(f). The current i_{Lk1} is dropped till zero. The magnetizing inductor L_m continuously transfers energy to the third leakage inductor L_{k3} and the capacitor C_2. The energies are discharged from C_1 and C_3 to the load. The current i_{d3} charges C_2 and supplies the load current.

III. Steady-State Analysis

In order to simplify the CCM steady-state analysis, the following factors are taken into account. All the leakage inductors of the coupled inductor are neglected, and all of components are ideal without any parasitic components. The voltages V_b, V_{C1}, V_{C2}, and V_{C3} are considered to be constant due to infinitely large capacitances.

A. Step-Up Gain

During the turn-on period of switch S, the following equations can be written as:

$$V_{C3} = V_{N3} = n_3 \cdot V_{\rm in} \tag{1}$$

$$V_{Cb} = V_{\rm in} + V_{N2} = (n_2 + 1) \cdot V_{\rm in}. \tag{2}$$

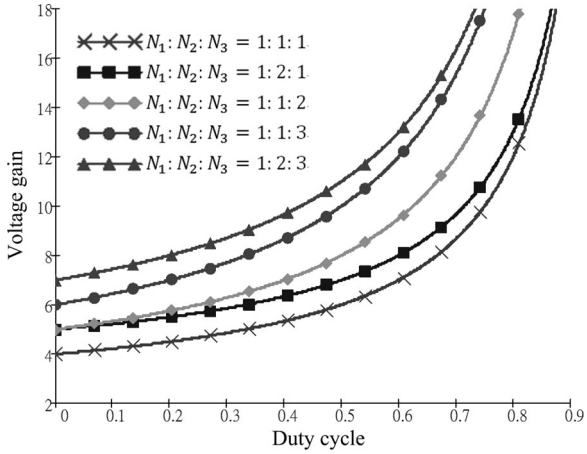

Fig. 6. Step-up gain versus duty ratio under various turns ratios.

During the turn-off period of switch S, the following equations can be expressed as:

$$V_{C2} = n_3 \left[V_{C1} - (2 + n_2) \cdot V_{\text{in}}\right] \tag{3}$$

$$V_{C1} = \left(\frac{D}{1-D} + 2 + n_2\right) \cdot V_{\text{in}}. \tag{4}$$

Thus, the output voltage V_O can be expressed as

$$V_O = V_{C1} + V_{C2} + V_{C3}. \tag{5}$$

By substituting (1), (3), and (4) into (5), the voltage gain of the proposed converter is given by

$$M_{\text{CCM}} = \frac{V_o}{V_{\text{in}}} = n_2 + \frac{2 - D + n_3}{1 - D}. \tag{6}$$

Equation (6) shows that high step-up gain can be easily obtained by increasing the turns ratio of the coupled inductor without large duty cycle. The step-up gain versus duty ratio under various turns ratios is plotted in Fig. 6.

B. Voltage Stress

The voltage stress on the main switch is given as follows:

$$M_S = \frac{V_{S1}}{V_{\text{out}}} = \frac{1}{2 - D + (1 - D)\, n_2 + n_3}. \tag{7}$$

When the switching S is turned OFF, the diodes D_1 and D_3 are reverse biased. Therefore, the voltage stresses of D_1 and D_3 are as follows:

$$M_{D1} = \frac{V_{D1}}{V_{\text{out}}} = \frac{1 + n_2}{2 - D + (1 - D)\, n_2 + n_3} \tag{8}$$

$$M_{D4} = \frac{V_{D3}}{V_{\text{out}}} = \frac{n_3}{2 - D + (1 - D)\, n_2 + n_3}. \tag{9}$$

When the switch S is in turn-on period and the diodes D_2 and D_3 are reverse biased. Therefore, the voltage stresses of diodes

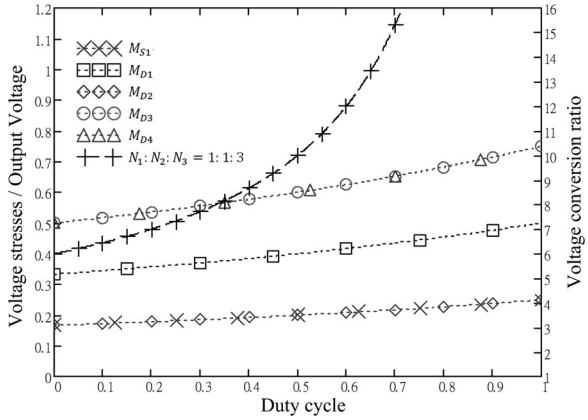

Fig. 7. Voltage stresses on the main switch and diodes.

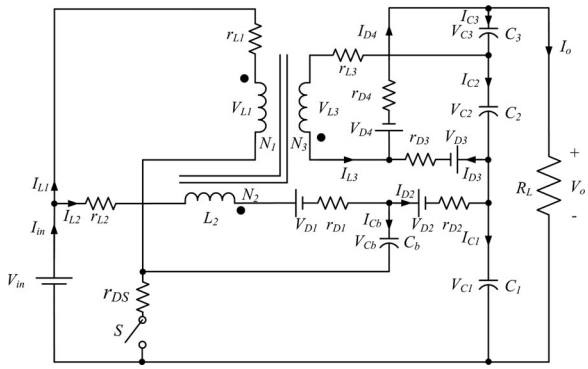

Fig. 8. Equivalent circuit including inductor conduction losses.

D_2 and D_3 are as follows:

$$M_{D2} = \frac{V_{D2}}{V_{\text{out}}} = \frac{1}{2 - D + (1 - D)\, n_2 + n_3} \tag{10}$$

$$M_{D3} = \frac{V_{D4}}{V_{\text{out}}} = \frac{n_3}{2 - D + (1 - D)\, n_2 + n_3}. \tag{11}$$

Equations (7)–(11) can be illustrated to determine the maximum voltage stress on each power drives. The voltage stress on the switch and diodes is plotted in Fig. 7.

C. Analysis of Conduction Losses

Some conduction losses are caused by resistances of semiconductor components and coupled inductor. Thus, all the components in the analysis of conduction losses are not continuously assumed to be ideal, except for all the capacitors. Diode reverse recovery problems, core losses, switching losses, and the ESR of capacitors are not discussed in this section. The characteristics of leakage inductor are disregarded because of energy recycling. The equivalent circuit, which includes the conduction losses of coupled inductors and semiconductor components, is shown in Fig. 8. The corresponding equivalent circuit includes copper resistances r_{L1}, r_{L2}, and r_{L3}, all the diode forward resistances r_{D1}, r_{D2}, r_{D3}, and r_{D4}, and the on-state resistance $R_{\text{DS-ON}}$ of the power switch.

Small-ripple approximation was used to calculate conduction losses and all currents that pass through components were

TABLE I
COMPARISON BETWEEN THREE-WINDING COUPLED INDUCTOR HIGH STEP-UP CONVERTERS

Converter Type	$M=\frac{V_{out}}{V_{in}}$	$M_S=\frac{V_{DS}}{V_{out}}$
Proposed converter	$n_2+\frac{2-D+n_3}{1-D}$	$\frac{1}{1+(n_2+n_3)\cdot D+n_2\cdot(1-D)}$
Converter in [37]	$n_3+\frac{1+(n_2+n_3)\cdot D}{1-D}$	$\frac{1}{1+n_3\cdot D+(1+n_3)\cdot(1+D)}$
Converter in [39]	$(1+n_2)+\frac{1+D\cdot n_3}{1-D}$	$\frac{1}{2-D+n_2\cdot(1-D)+n_3}$

approximated by the dc components. Thus, the magnetizing current and capacitor voltages are assumed to be constant. Finally, through voltage–second balance and capacitor-charge balance, the voltage conversion ratio with conduction losses can be derived from

$$\frac{V_o}{V_{\rm in}}=\frac{\left(n_2+\frac{2-D+n_3}{1-D}\right)-K}{1+\frac{\alpha}{R_L(1-D)^2}+\frac{r_{L3}}{R_L D(1-D)}+\frac{\beta}{R_L(1-D)}+\frac{\gamma}{R_L D}} \tag{12}$$

where

$$\begin{cases} K = \frac{V_{D1}+V_{D2}+V_{D3}+V_{D4}}{V_{\rm in}} \\ \alpha = (1+n_2)\,D\cdot r_{L1}+(1+n_3)\,D\cdot r_{\rm DS} \\ \beta = (1+2n_2+n_3)\,r_{L1}+r_{L3}+r_{D2}+r_{D3} \\ \quad +(2+n_2+2n_3)\,r_{\rm DS} \\ \gamma = r_{L2}+r_{D1}+r_{D4}+(1+n_2+n_3)\,r_{\rm DS} \end{cases}$$

Efficiency is expressed as follows:

$$\eta=\frac{V_{\rm in}-n_2+\frac{2-D+n_3}{1-D}\cdot(V_{D1}+V_{D2}+V_{D3}+V_{D4})}{V_{\rm in}+\frac{\alpha}{R_L(1-D)^2}+\frac{r_{L3}}{R_L D(1-D)}+\frac{\beta}{R_L(1-D)}+\frac{\gamma}{R_L D}}. \tag{13}$$

On the basis of (13), it can be inferred that the efficiency will be higher if the input voltage is substantially higher than the summation of the forward bias of all the diodes, or if the load is substantially larger than the resistances of coupled inductors and semiconductor components. In addition, the maximally effect for efficiency is duty cycle, and the secondary is copper resistance of the coupled inductor.

D. Comparison Between the Proposed Converter and the Other High Step-Up Converters

The performance of the proposed converter is verified by an analytical comparison with other three-winding coupled inductor high step-up converters for fuel cell, and it is assumed that all the converters are operated in CCM. Moreover, for the sake of fair comparison, the analysis will also assume that the input voltage and the turns ratios of coupled inductor are the same: $n_2=1.5$; $n_3=1.5$. Table I summarizes the voltage conversion ratio and the switch stress for the proposed converter and the other single switch high step-up converter topologies introduced in [37] and [39].

In this comparison between the proposed converter and other converter, n_2 is defined as the turns ratio N_2/N_1; and n_3 is defined as the turns ratio N_3/N_1.

Fig. 9 shows the comparison of voltage gain and the switch stress between the three-winding coupled inductor high step-up converters. Fig. 9(a) indicates that the voltage gain of the proposed converter is higher than that of the other high step-up converters at duty cycle of $0.1< D < 0.6$. Fig. 9(b) indicates that the voltage stress of switch of the proposed converter is lower than that of other high step-up converter at duty cycle of $0.1 < D < 0.6$. This is a very attractive feature because the low-voltage-rated MOSFET with lower $R_{\rm DS\text{-}ON}$ can be adopted to improve the efficiency. Under $D > 0.6$, although the voltage gain of the proposed converter is not the highest and the voltage stress of the proposed converter is not the lowest, the operation under large duty cycle $D > 0.6$ resulting in low efficiency will not be designed in reasonable consideration.

IV. DESIGN AND EXPERIMENTS OF THE PROPOSED CONVERTER

A. Design Guidelines

The PEMFC module consists of fuel cell stack of the PEM type, mechanical auxiliaries, and electronic control module. During normal operation, the generated voltage of fuel cell is related to load. Under full-load operation, the rated power is 2 kW and the corresponding voltage is 60 V, which is shown in Fig. 10. Also, the nominal parameter is shown in Table II.

The proposed high step-up converter is initially designed to convert the generated dc voltage from fuel cell stacks into 400 V. The required step-up conversion ratio is up to 6.7. Therefore, in order to make the duty cycle lower than 0.5 to decrease the conduction losses, the key design step is to determine the turns ratio of the coupled inductor. The relationship of duty cycle versus conversion efficiency and voltage gain under different turns ratios is shown in Fig. 11.

Thus, the turns ratio of the coupled inductor is set as 1:1:1.5. The magnetizing inductor can be designed based on the current ripple percentage of magnetizing inductor under full-load operation, and the related equations are given as

$$I_{Lm}=\frac{1+n_3}{1-D_{\max}}I_{o,\max} \tag{14}$$

$$L_m=\frac{V_{\rm in,min}\times D_{\max}}{f\times 2\Delta i_{Lm}} \tag{15}$$

The capacitors can be designed based on the voltage ripple percentage of capacitor under full-load operation, and the related equations are given as

$$C_1=C_3=\frac{I_{o,\max}\times D_{\max}}{f\times\Delta v_C} \tag{16}$$

$$C_b=C_2=\frac{I_{o,\max}}{f\times\Delta v_C} \tag{17}$$

B. Experimental Results

The proposed converter for fuel cell input source, prototype circuit is tested to verify the performance. The range of duty cycle D under input voltage 60–90 V is designed as 0.2–0.5 and the turns ratio n_1:n_2:n_3 is selected as 1:1:1.5. The leakage inductance L_{k1} is measured as 3.3 μH. All of the major

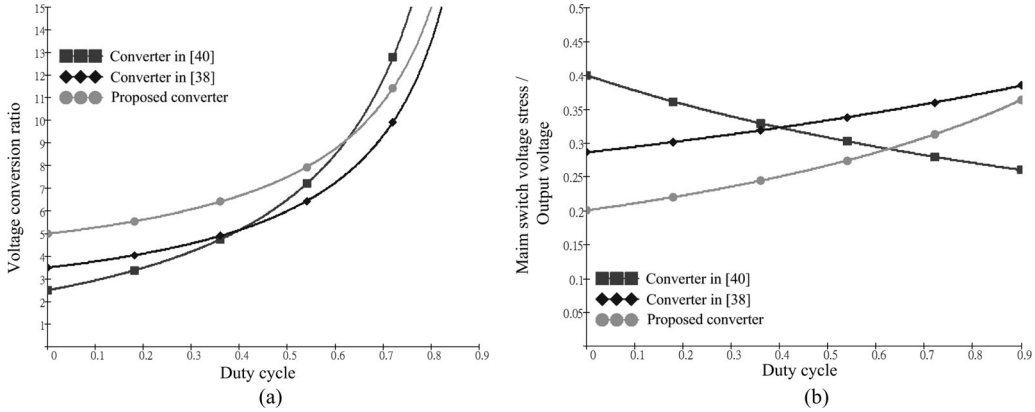

Fig. 9. (a) Voltage conversion ratios. (b) Normalized switch voltage stresses.

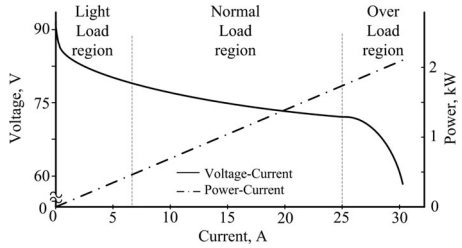

Fig. 10. Fuel cell polarization curves.

TABLE II
NOMINAL PARAMETERS OF PEMFC

PEMFC	Specifications
Rated voltage	72 V
Rated current	55 A
Voltage range	60 V~ 90V
Fuel cell efficiency	>50%
Hydrogen purity	>99.95%
Working pressure	0.7-0.8 bar
Ambient temperature	-5~ -40℃

components parameters of the prototype used for experiments are presented in Table III.

The experimental waveforms measured at full load 2 kW are shown in Fig. 12. The performance of the clamp feature is shown in Fig. 12(a). $V_{\rm GS}$ is the switch control signal. $V_{\rm DS}$ is the voltage stress across the MOSFET. $I_{\rm in}$ is the input current from full cell stacks. The voltage of $V_{\rm DS}$ is clamped at 120 V, which is smaller than output voltage 400 V. The characteristic is helpful in using a low-voltage-rated switch with low $R_{\rm DS\text{-}ON}$ for reducing the conduction losses. The currents i_{D1} charging switched capacitor C_b and i_{D2} through the clamp diode D_2 are shown in Fig. 12(b). The currents i_{D3} and i_{D4} of voltage doubler circuit are shown in Fig. 12(c). All diode voltage stresses V_{D1}, V_{D2}, V_{D3}, and V_{D4} are shown in Fig. 12(d) and (e), which are smaller than the output voltage, and can be demonstrated that the experimental results and theoretical analysis of diode voltage stresses correspond. Moreover, the phenomena of voltage oscillation can be eliminated, and thus, snubber circuits in the proposed converter schemes are not necessary.

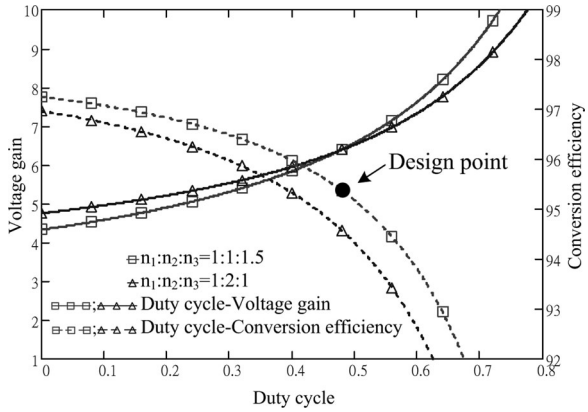

Fig. 11. Relationship of duty cycle and conversion efficiency under different turns ratios.

TABLE III
COMPONENTS PARAMETERS OF THE PROPOSED CONVERTER

Part		Specifications
Input DC voltage		60-90 V
Output DC voltage		400 V
Maximum output power		5 A
Switching frequency		50 kHz
Current Mode PWM Controller		UC3845
Coupled inductors turns ratio		N_1:N_2:N_3=1:1:1.5
Magnetizing inductor		170uH
Main power MOSFET		IXFN 130N30 300V, 130A, 22mΩ
Diodes	D_1	DSEP30-06A 600V, 30A
	$D_2/D_3/D_4$	MBR20200CT 200V, 20A
Capacitors	C_b	220uF/200V
	C_1	220uF/200V
	C_2/C_3	470uF/450V

Fig. 13 summarizes the conversion efficiency of the proposed converter and generated voltage of PEMFC versus output power. From the experimental results, the generated voltage of PEMFC decreases as the output power increases due to chemical polarization, concentration polarization, and resistance polarization

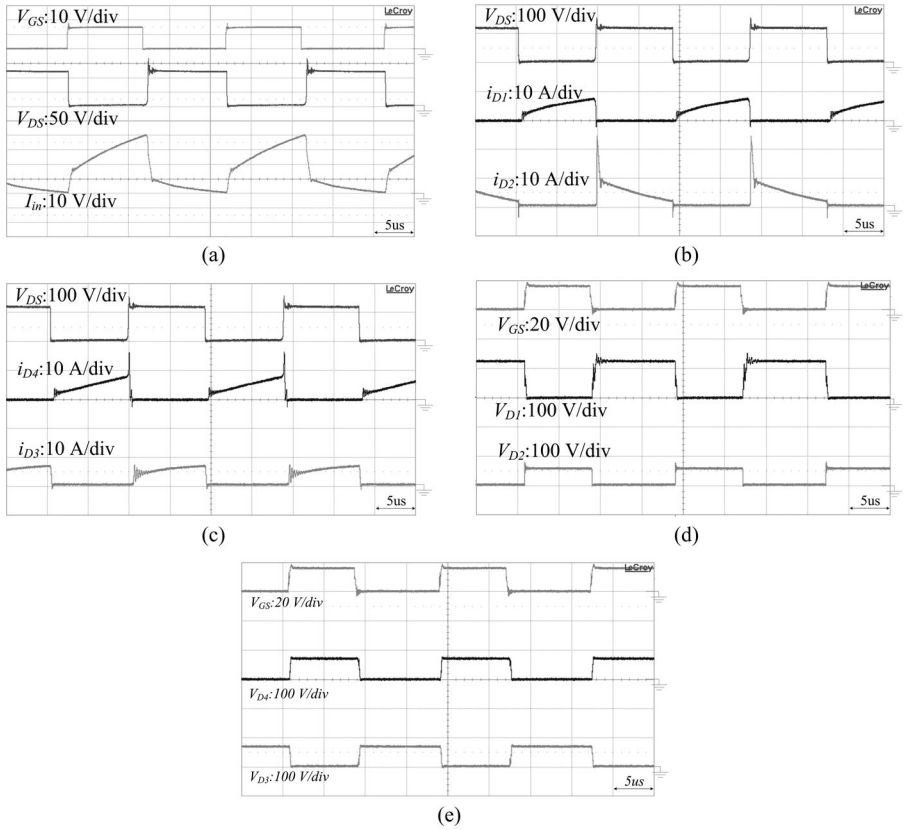

Fig. 12. Experimental waveforms measured at full load 2 kW.

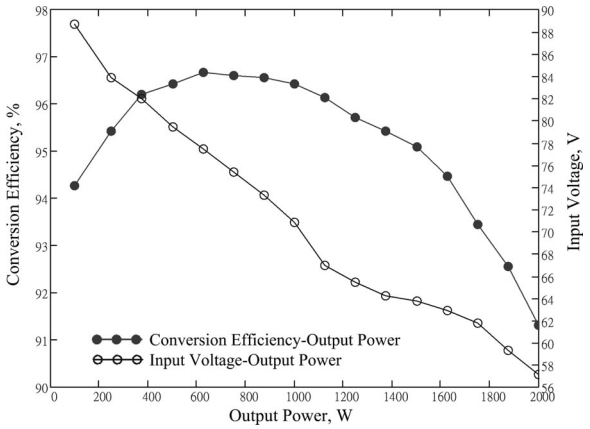

Fig. 13. Conversion efficiency and fuel cell voltage versus output power.

on voltages of fuel cells. The maximum conversion efficiency is 96.81%, and the full-load efficiency with lowest input voltage 57.1 V is 91.32%. Under no-load condition, the output voltage is 401.4 V, under half-load condition, the output voltage is 400.2 V, and under full-load condition, the output voltage is 398.5 V. The load regulation is lower than 1%.

V. Conclusion

In this paper, a high step-up dc–dc converter for fuel cell hydroid electric vehicle applications is clearly analyzed and successfully verified. By using technologies of three-winding coupled inductor, switched capacitor, and voltage doubler circuit, the high step-up conversion can be efficiently obtained. The leakage energy is recycled and large voltage spike is alleviated; thus, the voltage stress is limited and the efficiency is improved. The full-load efficiency is up to 91.32% and the maximum efficiency is up to 96.81%. The voltage stress on the main switch is clamped as 120 V at $D_{\max}$. The low-voltage-rated switch with low $R_{\mathrm{DS\text{-}ON}}$ can be selected for the reduction of conduction losses. Thus, the proposed converter is suitable for high-power applications as fuel cell systems in hydroid electric vehicles.

References

[1] W. Li, X. Lv, Y. Deng, J. Liu, and X. He, "A review of non-isolated high step-up DC/DC converters in renewable energy applications," in *Proc. IEEE Appl. Power Electron. Conf. Expo.*, Feb. 2009, pp. 364–369.

[2] W. Li and X. He, "Review of nonisolated high-step-up DC/DC converters in photovoltaic grid-connected applications," *IEEE Trans. Ind. Electron.*, vol. 58, no. 4, pp. 1239–1250, Apr. 2011.

[3] M. A. Laughton, "Fuel cells," *IEE Eng. Sci. Edu. J.*, vol. 11, no. 1, pp. 7–16, Feb. 2002.

[4] W. Jiang and B. Fahimi, "Active current sharing and source management in fuel cell-battery hybrid power system," *IEEE Trans. Ind. Electron.*, vol. 57, no. 2, pp. 752–761, Feb. 2010.

[5] P. Thounthong, S. Rael, and B. Davat, "Analysis of supercapacitor as second source based on fuel cell power generation," *IEEE Trans. Ind. Electron.*, vol. 24, no. 1, pp. 247–255, Mar. 2009.

[6] A. Khaligh and Z. Li, "Battery, ultracapacitor, fuel cell, and hybrid energy storage systems for electric, hybrid electric, fuel cell, and plug-in energy source applications: State of the art," *IEEE Trans. Veh. Technol.*, vol. 59, no. 6, pp. 2806–2814, Jul. 2010.

[7] L. Wang and H. Li, "Maximum fuel economy-oriented power management design for a fuel cell vehicle using battery and ultracapacitor," *IEEE Trans. Ind. Appl.*, vol. 46, no. 3, pp. 1011–1020, May/Jun. 2010.
[8] M. Marchesoni and C. Vacca, "New DC–DC converter for energy storage system interfacing in fuel cell energy source applications," *IEEE Trans. Power. Electron.*, vol. 22, no. 1, pp. 301–308, Jan. 2007.
[9] G.-J. Su and L. Tang, "A reduced-part, triple-voltage DC-DC converter for EV/HEV power management," *IEEE Trans. Power Electron.*, vol. 24, no. 10, pp. 2406–2410, Oct. 2009.
[10] S. M. Dwari and L. Parsa, "A novel high efficiency high power interleaved coupled-inductor boost DC–DC converter for hybrid and fuel cell electric vehicle," in *Proc. IEEE Veh. Power Propulsion Conf.*, Sep. 2007, pp. 399–404.
[11] P. Xuewei and A. K. Rathore, "Novel interleaved bidirectional snubberless soft-switching current-fed full-bridge voltage doubler for fuel cell vehicles," *IEEE Trans. Power Electron.*, vol. 28, no. 12, pp. 5535–5546, Dec. 2013.
[12] A. K. Rathore and U. R. Prasanna, "Analysis, design, and experimental results of novel snubberless bidirectional naturally clamped ZCS/ZVS current-fed half-bridge dc/dc converter for fuel cell vehicles," *IEEE Trans. Ind. Electron.*, vol. 60, no. 10, pp. 4482–4491, Oct. 2013.
[13] O. Hegazy, J. Van Mierlo, and P. Lataire, "Analysis, modeling, and implementation of a multidevice interleaved dc/dc converter for fuel cell hybrid electric vehicles," *IEEE Trans. Power Electron.*, vol. 27, no. 11, pp. 4445–4458, Nov. 2012.
[14] U. R. Prasanna, P. Xuewei, A. K. Rathore, and K Rajashekara, "Propulsion system architecture and power conditioning topologies for fuel cell vehicles," in *Proc. IEEE Energy Convers. Congr. Expo.*, pp. 1385–1392.
[15] Z. Zhang, Z. Ouyang, O. C. Thomsen, and M. A. E. Andersen, "Analysis and design of a bidirectional isolated dc–dc converter for fuel cells and supercapacitors hybrid system," *IEEE Trans. Power Electron.*, vol. 27, no. 2, pp. 848–859, Feb. 2012.
[16] P. F. Ksiazek and M. Ordonez, "Swinging bus technique for ripple current elimination in fuel cell power conversion," *IEEE Trans. Power Electron*, vol. 29, no. 1, pp. 170–178, Jan. 2014.
[17] R. W. Erickson and D. Maksimovic,, *Fundamentals of Power Electronics*, 2nd ed. New York, NY, USA: Springer, 2001.
[18] A. I. Pressman, K. Billings, and T. Morey, *Switching Power Supply Design*, 3rd ed. New York, NY, USA: McGraw-Hill, 2009.
[19] S. J. Finney, B. W. Williams, and T. C. Green, "RCD snubber revisited," *IEEE Trans. Ind. Appl.*, vol. 32, no. 1, pp. 155–160, Jan./Feb. 1996.
[20] W. K. Thong and C. Pollock, "A novel low-cost RCD snubber for bifilar-wound motors," *IEEE Trans. Ind. Appl.*, vol. 38, no. 3, pp. 688–694, May/Jun. 2002.
[21] M. Serine, A. Saito, and H. Matsuo, "High efficiency DC/DC converter circuit using charge storage diode snubber," in *Proc. 29th Int. Telecommun. Energy Conf.*, 2007, pp. 355–361.
[22] K. B. Park, G. W. Moon, and M. J. Youn, "Nonisolated high step-up stacked converter based on boost-integrated isolated converter," *IEEE Trans. Power Electron.*, vol. 26, no. 2, pp. 577–587, Feb. 2011.
[23] H. Xiao and S. Xie, "A ZVS bidirectional DC–DC converter with phase-shift plus PWM control scheme," *Proc. Appl. Power Electron. Conf.*, vol. 23, no. 2, pp. 813–823, Mar. 2008.
[24] P. Dos Santos, G. Giacomini, J. S. Scholtz, and M. Mezaroba, "Step-up/step-down DCDC ZVS PWM converter with active clamping," *IEEE Trans. Ind. Electron.*, vol. 55, no. 10, pp. 3625–3643, 2008.
[25] M. D. Seeman and S. R. Sanders, "Analysis and optimization of switched-capacitor DC–DC converters," *IEEE Trans. Power Electron.*, vol. 23, no. 2, pp. 841–851, Mar. 2008.
[26] F. L. Luo, "Six self-lift DC-DC converters, voltage lift technique," *IEEE Trans. Ind. Electron.*, vol. 48, no. 6, pp. 1268–1272, Dec. 2001.
[27] F. L. Luo and H. Ye, "Positive output super-lift converters," *IEEE Trans. Ind. Electron.*, vol. 18, no. 1, pp. 105–113, Jan. 2003.
[28] F. L. Luo and H. Ye, "Positive output multiple-lift push-pull switched-capacitor Luo-converters," *IEEE Trans. Ind. Electron.*, vol. 51, no. 3, pp. 594–602, Jun. 2004.
[29] Q. Zhao and F. C. Lee, "High-efficiency, high step-up DC-DC converters," *IEEE Trans. Ind. Electron.*, vol. 18, no. 1, pp. 65–73, Jan. 2003.
[30] K. C. Tseng and T. J. Liang, "Novel high-efficiency step-up converter," *Proc. Inst. Elect. Eng.-Elect. Power Appl.*, vol. 151, no. 2, pp. 182–190, Mar. 2004.
[31] T. J. Liang and K. C. Tseng, "Analysis of integrated boost-flyback step-up converter," *Proc. Inst. Elect. Eng.-Elect. Power Appl.*, vol. 152, no. 2, pp. 217–225, Mar. 4, 2005.
[32] J. W. Baek, M. H. Ryoo, T. J. Kim, D. W. Yoo, and J. S. Kim, "High boost converter using voltage multiplier," in *Proc. 31st Ann. Conf. IEEE Ind. Electron. Soc.*, Raleigh, NC, USA, Nov. 2005, pp. 567–572.
[33] E. H. Ismail, M. A. Al-Saffar, and A. J. Sabzali, "High conversion ratio DC–DC converters with reduced switch stress," *IEEE Trans. Ind. Electron.*, vol. 55, no. 7, pp. 2139–2151, Aug. 2008.
[34] K. C. Tseng, C. C. Huang, and W. Y. Shih, "A high step-up converter with a voltage multiplier module for a photovoltaic system," *IEEE Trans. Power Electron.*, vol. 28, no. 6, pp. 3047–3057, Jun. 2013.
[35] K. C. Tseng and C. C. Huang, "High step-up high-efficiency interleaved converter with voltage multiplier module for renewable energy system," *IEEE Trans. Ind. Electron.*, vol. 61, no. 3, pp. 1311–1319, Mar. 2014.
[36] R. J. Wai and K. Y. Duan, "High step-up converter with coupled-inductor," *IEEE Trans. Power. Electron.*, vol. 20, no. 5, pp. 1025–1035, Sep. 2005.
[37] R. J. Wai and K. Y. Duan, "High-Efficiency DC-DC converter with high voltage gain and reduced switch stress," *IEEE Trans. Power Electron.*, vol. 54, no. 1, pp. 354–364, Feb. 2007.
[38] L. S. Yang, T. J. Liang, and J. F. Chen, "Transformer less DC–DC converters with high step-up voltage gain," *IEEE Trans. Ind. Electron.*, vol. 56, no. 8, pp. 3144–3152, Aug. 2009.
[39] S. K. Changchien, T. J. Liang, J. F. Chen, and L. S. Yang, "Novel high step-up DC–DC converter for fuel cell energy conversion system," *IEEE Trans. Ind. Electron.*, vol. 57, no. 6, pp. 2007–2017, Jun. 2010.

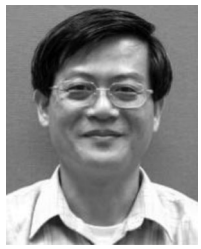

Kuo-Ching Tseng was born in Tainan, Taiwan, in 1957. He received the M.S. degree in electrical engineering from Da-Yeh Polytechnic Institute, Chang Hua, Taiwan, in 1999, and the Ph.D. degree in electrical engineering from National Cheng Kung University, Tainan, in 2004.

From July 1988 to 1996, he was an R & D Engineer with Lumen Co., Ltd., Taiwan, working on UPSs and switching power supply design. In February 2003, he joined the Department of Electrical Engineering, Da-Yeh Institute of Technology. Since 2008, he has been with the Department of Electronic Engineering, National Kaohsiung First University of Science and Technology, Kaohsiung, Taiwan, where he is currently an Associate Professor. His current research interests include dc/dc converters and power-factor correction techniques, power management control system design, solar energy conversion system design, switching power converter design, and renewable energy conversion system design.

Dr. Tseng received the Electric Power Applications Premium paper entitled "*Novel High-Efficiency Step-Up Converter*" from the Institution of Electrical Engineers in 2004/2005.

Jang-Ting Lin was born in Nantou, Taiwan, in 1986. He received the B.S. degrees in electronics engineering from the National Kaohsiung First University of Science and Technology, Kaohsiung, Taiwan, in 2012, where he is currently working toward the M.S. degree.

His research interests include power electronics and energy conversion.

Chi-Chih Huang was born in Pingtung, Taiwan, in 1989. He received the B.S. degree in electronics engineering from the National Kaohsiung First University of Science and Technology, Kaohsiung, Taiwan, in 2011, where he is currently working toward the M.S. degree.

His research interests include power electronics and energy conversion.

Mr. Huang received the Recognition of Excellence for research in the field of smart grid and green electronics in the 2013 International Symposium on Next-Generation Electronics. He has participated in manuscript review for the IEEE TRANSACTIONS ON POWER ELECTRONICS.